communications earth & environment

ARTICLE

https://doi.org/10.1038/s43247-024-01212-1 OPEN

Projected amplification of summer marine heatwaves in a warming Northeast Pacific Ocean

Marylou Athanase [1]✉, Antonio Sánchez-Benítez[1], Helge F. Goessling [1], Felix Pithan [1] & Thomas Jung [1,2]

Marine heatwaves are expected to become more frequent, intense, and longer-lasting in a warming world. However, it remains unclear whether feedback processes could amplify or dampen extreme ocean temperatures. Here we impose the observed atmospheric flow in coupled climate simulations to determine how the record-breaking 2019 Northeast Pacific marine heatwave would have unfolded in preindustrial times, and how it could unravel in a +4 °C warmer world compared to present-day conditions. We find that air-sea interactions, involving reductions in clouds and ocean mixed-layer depth and air advection from fast-warming subpolar regions, modulate warming rates within the marine heatwave. In a +4 °C warmer climate, global oceans are +1.9 °C warmer than present levels, and regional mean warming in the Northeast Pacific can reach +2.3–2.7 ± 0.25 °C. Our identified feedback processes are projected to further amplify the intensity and spatial extent of analogous Northeast Pacific summer marine heatwaves beyond those thresholds, with a warming reaching +2.9 ± 0.15 °C above present levels. Such an event-specific amplification would place even greater stress on marine ecosystems and fisheries.

[1] Alfred Wegener Institute, Helmholtz-Centre for Polar and Marine Research, Bremerhaven, Germany. [2] Institute of Environmental Physics, University of Bremen, Bremen, Germany. ✉email: marylou.athanase@awi.de

Heatwaves in the ocean, so-called marine heatwaves, are on the rise – like their atmospheric counterparts. A prominent recent marine heatwave occurred in summer 2019 in the Northeast Pacific Ocean. During June to August, sea surface temperatures (SST) reached an all-season record in local absolute SST[1], with summer SST anomalies (SSTAs) peaking at 2.5 °C above the 1984–2014 normal (Fig. 1a). The amplitude of this event was reminiscent of the historical 2013–2014 winter marine heatwave[2], which had devastating impacts on marine organisms[3–6] and contributed to severe droughts along the North-American west coast[7,8]. In summer, high ocean temperatures threaten local marine species if their thermal tolerances are exceeded, highlighting the importance of studying warm-season marine heatwaves. Preliminary surveys, for example, have linked the extreme 2019 temperatures to a crash of the Bering Sea snow crab stock in 2022[9]. Such consequences of North Pacific marine heatwaves on ecosystems[10–12], continental weather, or fishery economics[13,14], call for a better understanding of these phenomena and their changes in a warming world.

Several factors contributed to the development of the summer 2019 marine heatwave. A prolonged weakening of the North Pacific high-pressure system, probably associated with a positive phase of the El Niño-Southern Oscillation[15,16], resulted in weaker surface winds and led to a decrease in wind-driven upper ocean mixing[1]. In response, the mixed layer depth (MLD) was strongly reduced. Therefore, the downward atmospheric heat fluxes were absorbed by an anomalously thin mixed layer, explaining part of the intense ocean surface warming[17]. Furthermore, the reduced low-cloud cover over the Northeast Pacific[1] reinforced the marine heatwave by enabling increased downward shortwave radiation to reach the ocean surface[18,19].

The occurrence of such an extreme event usually raises at least two key questions:

- Was the extreme event influenced by anthropogenic climate change?
- How would the extreme event unfold in an even warmer climate?

The first enquiry is considered an attribution problem, while the second involves climate projections. For attribution and projections, two components of the total climate change signal can be distinguished: (i) the regional (and seasonal-) long-term mean temperature change (regional mean change, hereafter), which can depart from the (seasonal-) global-mean sea surface temperature (GMSST) increase; and (ii) the event-specific temperature change that involve local processes and can either enhance or dampen the regional mean warming signal (event-specific amplification or dampening, hereafter). This decomposition is well established for atmospheric heatwaves over land, where there is evidence that positive feedbacks related to soil moisture and evaporation can amplify the total warming of continental summer heatwaves above the expected (seasonal) global[20] and regional mean warming[21]. Our study examines whether corresponding air-sea mechanisms, e.g., related to upper-ocean dynamics, play a critical role in marine heatwaves.

Attribution of extreme events such as the 2019 marine heatwave traditionally relies on statistical or probabilistic approaches focusing on changes in frequency, duration, and intensity between past, present, and projected future climates[22,23]. Such studies conclude that SSTs similar to those reached in summer 2019 have become much more likely over the past century as a consequence of the increase in GMSST and Northeast Pacific

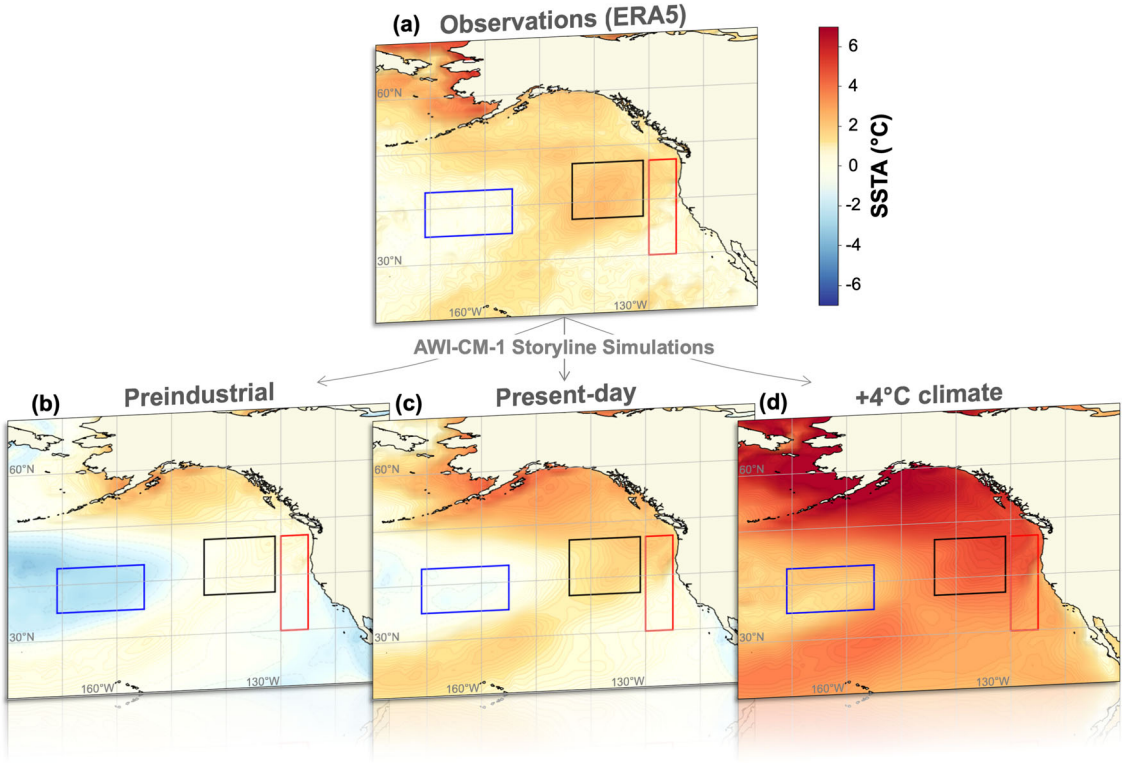

Fig. 1 The summer marine heatwave of 2019 if it unfolded in different climates. Summer SST anomalies (SSTA, in °C) with respect to the 1984–2014 climatology from (**a**) ERA5 observations data in 2019, and from (**b**–**d**) corresponding AWI-CM-1 nudged storyline simulations (5-member ensemble mean). Panels **b**–**d** represent the simulated marine heatwave if it would have unfolded with the same atmospheric flow as observed in 2019, but in (**b**) preindustrial, (**c**) present-day, and (**d**) +4 °C warmer climates. Contours are every 0.1 °C for positive values (solid lines), every 0.5 °C for negative values (dashed lines). The marine heatwave core (black box), coastal region (red box) and central North Pacific area (blue box) are indicated.

Ocean temperatures resulting from anthropogenic global warming[22–25]. To provide statistically significant statements, probabilistic methods rely on comprehensive observational datasets and large ensembles of climate model simulations[25–29]. Observations-based assessments can only contribute to addressing the attribution problem, and model projections usually require a large sample size[30] and high computational costs. Moreover, defining physical quantities, spatiotemporal boundaries, and thresholds that capture a given extreme event in a meaningful way is a challenge in probabilistic studies. This approach may also imply clustering diverse subtypes of events, for example associated with different circulation regimes, that respond differently to climate change.

Here, we employ an alternative approach in which a coupled climate simulation is nudged to observations of the temporal evolution of winds in the free troposphere, including the jet stream, while letting all other aspects (e.g., temperature, moisture, clouds, sea ice, and the ocean) evolve freely[31]. In these so-called storyline simulations, for brevity referred to as storylines hereafter, such wind nudging is applied using different climate boundary conditions (e.g., preindustrial and present-day, see Methods). The storylines therefore provide a novel way to generate close analogues of recently observed atmosphere-driven extreme events if they were to unfold in different background climates[21,32]. In contrast with traditional free-running simulations, which include potential changes in both dynamics and thermodynamics, the storyline approach thus imposes the dynamics to isolate the thermodynamic effects of climate change[33–35]. Consequently, this approach notably reduces uncertainties related to the inherent natural variability of the atmosphere[36–38] and produces a high signal-to-noise ratio at a low computational cost. Finally, storylines provide a powerful tool to make climate change tangible for non-expert citizens and to inform adaptation measures.

We apply this storyline approach to an extreme oceanic event –for the first time to the best of our knowledge– and examine analogues of the summer 2019 North Pacific marine heatwave in past, present and future climates (Fig. 1b–d). We employ simulations based on the medium-resolution ocean-atmosphere coupled climate model AWI-CM-1-MR[39–41] (AWI-CM-1 hereafter), which has contributed to phase 6 of the Coupled Model Intercomparison Project (CMIP6)[42] in support of the sixth IPCC Assessment Report[43]. We use two types of AWI-CM-1 coupled simulations, each comprising five ensemble members: free runs, which simulate the climate from 1850 to 2100 with natural and anthropogenic forcings; and the nudged storyline simulations, spawned using initial states from the free runs and in which the observed wind evolution from 2017 to 2020 is imposed (see Methods). Different background climate conditions in the nudged storylines are generated by using initial states and climate forcings from the free runs corresponding to preindustrial, present-day, and +4 °C warmer climates. The free-running and nudged configurations – both extensively validated[21,41,44] – thus only differ by their winds. Differences between the nudged storyline simulations and the free-run climatology therefore reveal the signal directly attributable to the specific conditions of the nudged atmospheric flow.

Unlike most previous storyline studies based on the nudging approach, which have used atmosphere-only models[35,45], we take advantage of the fully coupled nudged storyline simulations[21] to enable the direct reproduction of marine heatwaves and associated air-sea interactions (see Methods). The coupled storylines constitute a step forward for the understanding of the processes driving the evolution of marine heatwaves in a warming world.

Results

Present-day climate. In storyline simulations for present-day conditions, the model is nudged toward the evolution of free-tropospheric winds observed in 2017–2020 using reanalysis data (ERA5). These nudged coupled climate simulations create a realistic spatio-temporal analogue of the Northeast Pacific marine heatwave observed in summer 2019 (Figs. 1c and 2). Indeed, the weakened North Pacific high and associated reduced surface winds, dominant drivers of the summer 2019 marine heatwave[1], are well represented in the storyline simulations (Supplementary

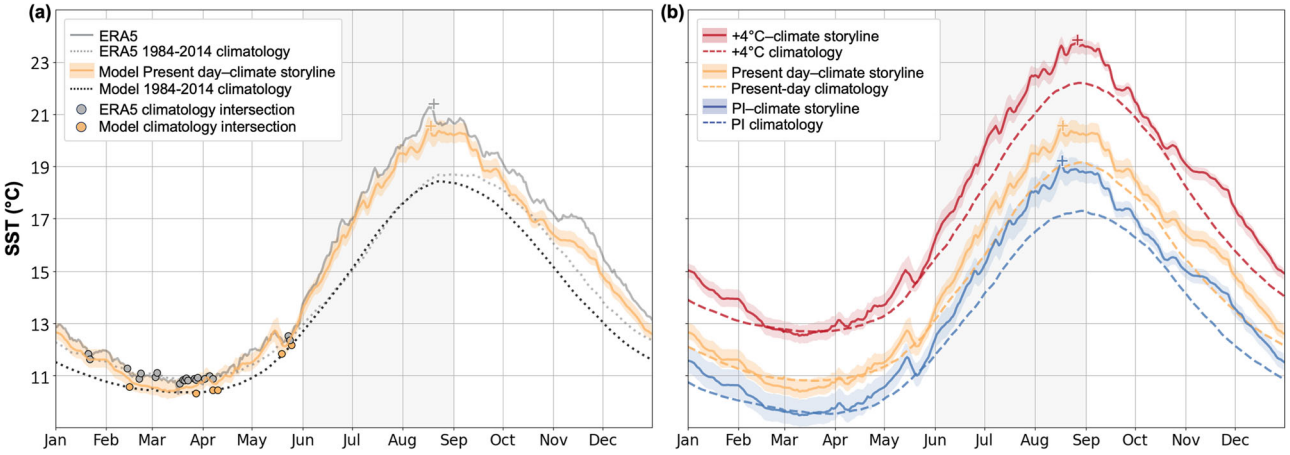

Fig. 2 Marine heatwave core temperature in different climates. Time series of SSTs (°C) in the marine heatwave core area (black box in Fig. 1). **a** SSTs in 2019 from ERA5 data (solid grey line), and from the present-day nudged storyline simulations (solid yellow line). The ERA5 and model climatology for the 1984–2014 reference period, used to derive anomalies shown in Fig. 1, are in grey and black dotted lines, respectively. Intersection with the climatology is indicated with circle markers. **b** Same for nudged storyline simulations of the marine heatwave if the same atmospheric flow unfolded in PI, present-day, and +4 °C climates (in solid blue, yellow and red lines, respectively). The corresponding model climatologies are in dashed lines (see Methods). The annual maximum is marked with a cross for ERA5 data and for nudged storyline simulations. Shaded envelopes are the ensemble range of storyline simulations. The summer season (June-to-August) is grey-shaded. All model climatologies are derived from the multidecadal free-running AWI-CM-1 simulations (see Methods).

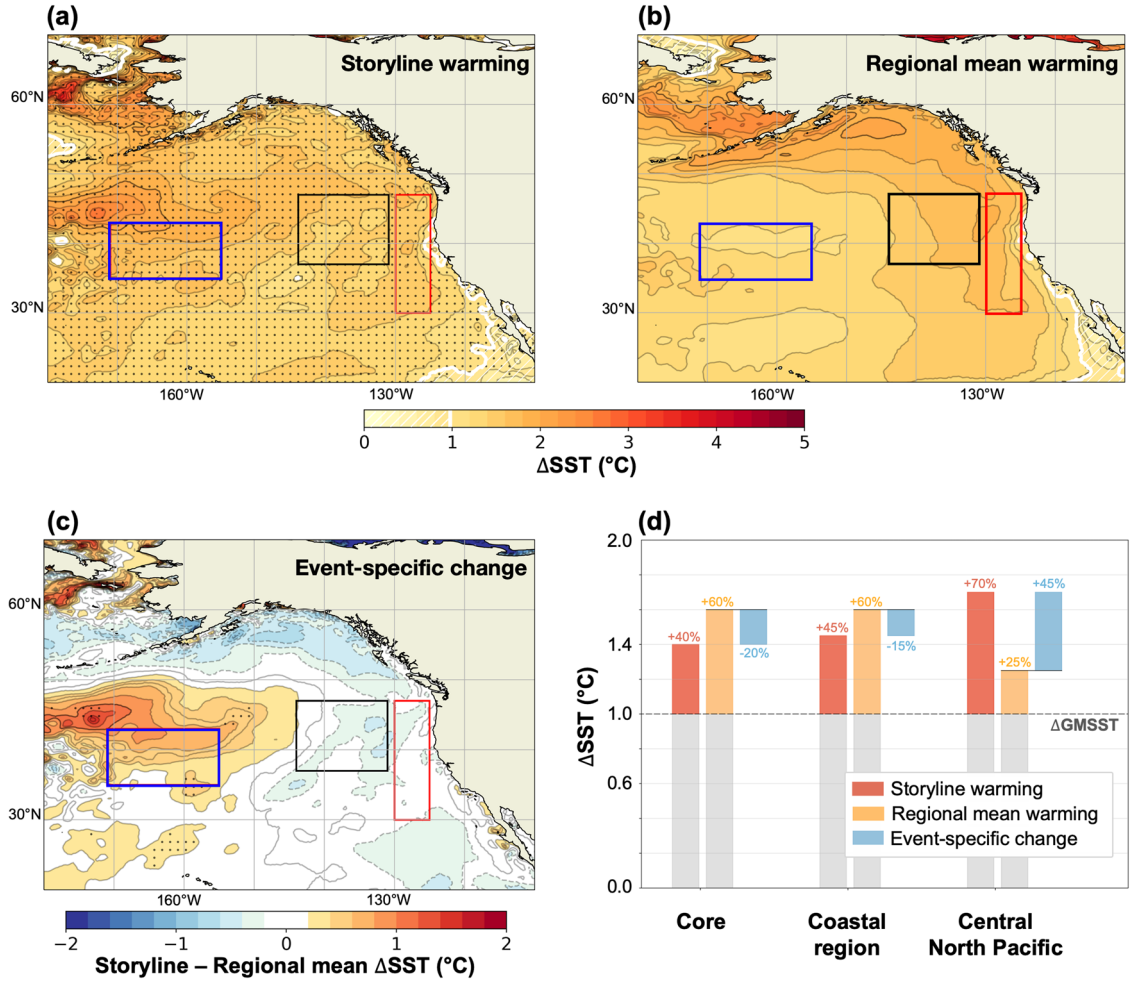

Fig. 3 Attribution of the marine heatwave to thermodynamical climate change. Summer SST (°C) changes between present-day and PI climates, derived (**a**) from the nudged storyline simulations (storyline warming) and (**b**) from the climatological-mean states in the free-running simulations (regional mean change). In **a** and **b**, values below the summer GMSST increase of 1 °C (white contour) are in white hatching. **c** Difference between storyline and regional mean warming, indicating the event-specific change in SSTs. Non-overlapping storyline ensembles in **a** and non-overlapping storyline warming and regional mean warming in **c** are in dotted areas (i.e., highly significant signal, see Methods). **d** Area-averaged SST change (°C) between present-day and PI climates, in the marine heatwave core (black box), coastal region (red box) and central North Pacific (blue box). The storyline change (red bars) is the total marine heatwave change signal, and results from the combined regional mean and event-specific changes (yellow and blue bars respectively). Values below the 1 °C summer GMSST change are grey-shaded.

Fig. 1). In response to the anomalous wind conditions, the simulations capture the particularly shallow summer MLD and reduced low-cloud cover[1,17], resulting in enhanced warming by strongly positive net shortwave radiation fluxes to the mixed layer (Supplementary Fig. 1 and 2). The associated horseshoe-like pattern of positive SSTAs is consequently well reproduced (Fig. 1c). Variations of daily SST in the marine heatwave core also closely resemble observations, with marine heatwave conditions emerging simultaneously in late May (Fig. 2). This is supported by a Pearson correlation coefficient of 0.93 and a *p*-value below 0.0001 for the year 2019, after removal of the respective ERA5 and model climatological mean seasonal cycles (dotted lines in Fig. 2a, see Methods). Therefore, our results show that nudging free-tropospheric winds is an effective method to capture the observed weather-driven marine extreme event in space and time.

Simulated summer SSTAs in the Gulf of Alaska northward of the marine heatwave are up to 2 °C larger than observed, while they are underestimated by 1 °C on average in the marine heatwave core (Fig. 1c), due to cold and warm biases, respectively, in the 1984–2014 model climatology (Supplementary Fig. 3). Indeed, CMIP6 models such as AWI-CM-1 have been shown to generally underestimate marine heatwave intensity, with coarse ocean resolutions and associated lack of small-scale features being one possible explanation[46].

Storyline attribution. After having established the approach's effectiveness, we use nudged storyline simulations to assess the effect of past and present anthropogenic climate change on the summer 2019 marine heatwave. The same anomalous atmospheric circulation – imposed in a preindustrial (PI) climate – leads to similar spatial patterns and temporal variations of ocean temperatures as the present-day event (Figs. 1b and 2). However, the anthropogenic warming causes much higher ocean temperatures during the present-day event than during a PI analogue, with maximum SSTs of 20.4 °C instead of 19.0 °C in the marine heatwave core (Fig. 2b). Differences between storyline simulations in different climates indicate the total summer warming signal within analogues of the marine heatwave, and are called storyline warming hereafter (see Methods). Between present and PI climates, the rise in summer SSTs is ubiquitous in the entire Northeast Pacific (Fig. 3a), but not uniform. The storyline

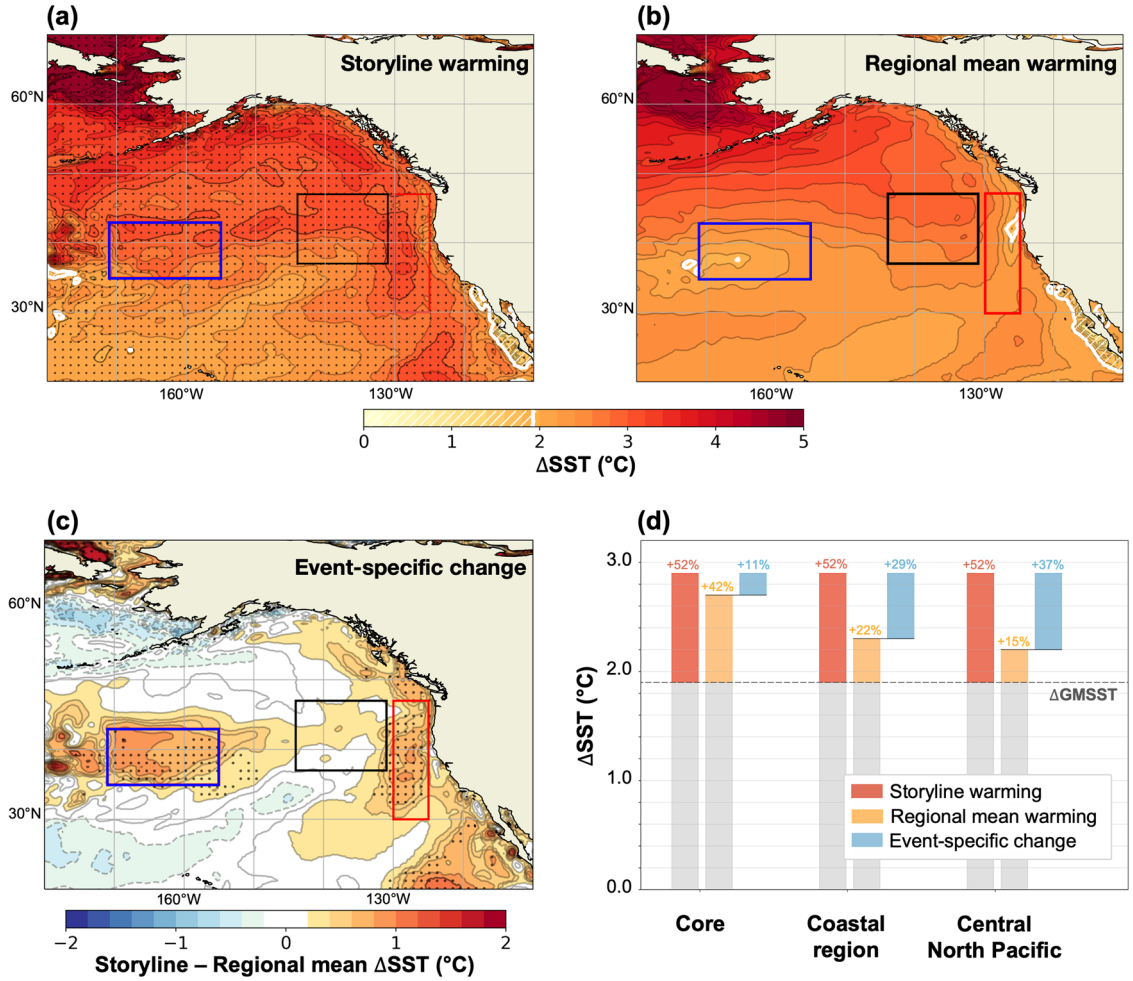

Fig. 4 Projection of the marine heatwave in a +4 °C warmer climate. Same as Fig. 3 for summer SST(°C) changes between +4 °C and present-day climates. In **a** and **b**, values below the summer GMSST increase of 1.9 °C (white contour) are in white hatching. **c** Event-specific change in SSTs. Non-overlapping storyline ensembles in **a** and non-overlapping storyline warming and regional mean change in **c** are in dotted areas (i.e., highly significant signal, see Methods). **d** Area-averaged SST change (°C) between +4 °C and present-day climates, in the marine heatwave core (black box), coastal region (red box) and central North Pacific (blue box). The storyline change (red bars) is the total marine heatwave change signal, and results from the combined regional mean and event-specific changes (yellow and blue bars respectively). Values below the 1.9 °C summer GMSST projected change are shaded in grey.

warming reaches 1.4 ± 0.2 °C in the marine heatwave core and coastal region, and is even more pronounced in the central North Pacific, totalling 1.7 ± 0.2 °C (Fig. 3a). This latter region experienced near-neutral SSTAs (Fig. 1a, c) and was thus not affected by the heatwave; but the storyline warming signal is distinct and strong, with no overlap between ensemble members for PI and the present-day conditions, implying a high signal-to-noise ratio (Figs. 2b and 3a; see Methods). The storyline warming in the Northeast Pacific marine heatwave is notably larger than what is expected from the global-mean rise in ocean surface temperature. Indeed, the free-running simulations indicate a summer GMSST increase limited to 1 °C between PI and present-day climates (Fig. 3a). The storyline warming signal is therefore substantially greater than the GMSST increase, from 40% larger in the marine heatwave to 70% larger in the central North Pacific (Fig. 3d).

The question arises whether the storyline warming is solely attributable to the regional mean summer warming, or whether the event-specific processes specific to the summer 2019 extreme conditions are amplifying or dampening the warming. We derive the climatological, regional mean summer warming from the free-running simulations (Fig. 3b, see Methods). The differences between the storyline warming and this climatological regional mean warming indicate the amplifying or dampening impact of event-specific processes (Fig. 3c, d).

The amplitude of the PI-to-present storyline warming in the marine heatwave core and coastal regions is primarily attributable to the regional mean climatological warming (Fig. 3b). The latter reaches 1.6 ± 0.2 °C, which is 60% larger than the GMSST increase, in agreement with observation-based estimates[25]. The local storyline warming (Fig. 3c) is 1.4–1.45 ± 0.2 °C in these two regions, suggesting event-specific processes may have even dampened the storyline warming below the regional mean warming by up to 0.2 ± 0.25 °C (Fig. 3d). However, in the central North Pacific region, the regional mean warming is more moderate and about 1.25 ± 0.3 °C (Fig. 3b). This indicates that in this region peripheral to the marine heatwave, the local storyline warming is dominated by a strong event-specific amplification of 0.45 ± 0.35 °C (Fig. 3c, d).

Storyline projection. Our simulations also provide insights on how the summer 2019 marine heatwave might unfold in warmer climates. In a +4 °C warmer world, the summer of 2019 atmospheric circulation would lead to SSTs in the Northeast Pacific that are 2–3 °C warmer than for present-day conditions (Fig. 4a),

and 4.3 °C warmer than in PI times. Maximum SSTs in the marine heatwave core are projected to reach 23.7 °C in late August, which is 3.3 ± 0.15 °C warmer than present, and 4.7 ± 0.15 °C warmer than PI analogues without anthropogenic climate change (Fig. 2b). The complete lack of overlap between ensemble members for the different climates highlights the robustness of these findings (Figs. 2b and 4a). Our results also suggest that the marine heatwave peak intensity would occur more than a week later when compared to present and PI analogues, prolonging risks into the late summer season (Fig. 2b).

The summer temperatures in the marine heatwave core, coastal region, and in the central North Pacific are projected to rise by 2.9 ± 0.15 °C on average (Fig. 4d). This is 1 °C higher, or 52% warmer than the projected 1.9 °C increase in the simulated GMSST. A comparison between the +4 °C-world summer warming in regional mean states and in our storyline simulations allows us to examine whether event-specific processes contribute to amplifying or dampening the predicted regional mean warming (Fig. 4).

Our free-running simulations project an above-average regional mean summer warming in the Northeast Pacific Ocean, which is more pronounced in sub-polar regions (Fig. 4b). The marine heatwave core location experiences a regional mean SST increase of 2.7 ± 0.2 °C, therefore dominating the storyline warming signal while event-specific processes contribute only to a moderate additional 0.2 ± 0.2 °C warming (Fig. 4c, d). However, a notable event-specific warming amplification is found to the west and east of the marine heatwave core (Fig. 4c). Indeed, the coastal region and the central North Pacific experience a more moderate regional mean warming of 2.3 ± 0.15 °C and 2.2 ± 0.25 °C on average, respectively, thus departing from the GMSST increase by 0.4 °C and 0.3 °C (Fig. 4b, d). Event-specific changes therefore lead to an average additional warming of 0.6 ± 0.2 °C and 0.7 ± 0.3 °C in future marine heatwave analogues, above the projected regional mean warming (Fig. 4c, d). Note that the event-specific warming amplification is particularly robust, with no overlap between the local storyline and regional mean warming, indicating a high signal-to-noise ratio (dotted areas in Fig. 4c; see Methods). By amplifying the warming more strongly at the marine heatwave periphery, event-specific processes overall contribute to a lateral expansion of marine heatwave analogues in a +4 °C world compared to the present-day event.

Drivers of marine heatwave changes. Which processes drive the warming amplification or dampening within the marine heatwave core, coastal region and central North Pacific? To address this question, we derive changes in mixed layer heat budget[1,47] within analogues of the marine heatwave (storyline change) and those expected from local climatological mean changes (regional mean change). We estimate the mixed layer budget-driven warming by considering only contributions from surface forcing processes, that is, how changes in surface heat fluxes absorbed in the mixed layer affect local temperature changes (Fig. 5a–c, see Methods for the complete analysis). Contributions from ocean dynamical processes, via horizontal advection and vertical entrainment, are treated as a residual term[1,17]. Anomalously shallow MLDs enhanced the marine heatwave, and the warming climate favours mixed layer shoaling[1,17,48]. It is therefore important to assess whether event-specific changes in budget-driven warming (blue bars, Fig. 5a–c) – which in turn contribute to local event-specific warming amplification or dampening – are driven by changes in the anomalous MLD or by changes in the surface heat flux itself[49,50]. We further decompose the event-specific change in mixed layer budget-driven warming into two contributions: from event-specific changes in net surface heat flux only; and from event-specific changes in MLD only (Fig. 5d, see Methods). They are referred to as Flux-varying contribution and MLD-varying contribution hereafter, respectively.

Between PI and present-day storyline simulations of the marine heatwave, changes in surface heat fluxes absorbed in the mixed layer are insufficient to explain the event-specific temperature changes in Fig. 3d (see Supplementary Note, Supplementary Figs. 5 and 6). Such disparities suggest that ocean dynamical processes likely play an important role in modulating the warming, in particular for regions at the periphery of the marine heatwave where mixed layers are relatively deeper. Contributions from oceanic advection and entrainment are quantified as a residual term here, and we propose potential driving mechanisms in the discussion.

In contrast, in a +4 °C warmer world the projected marine heatwave warming amplification primarily results from changes in surface heat fluxes absorbed in the mixed-layer (Fig. 5). Indeed, our storyline simulations exhibit enhanced mixed layer budget-driven warming from net surface fluxes Q_{net}, exceeding the projected regional mean changes. The associated excess warming (blue bars, Fig. 5a–c) is on the same order of magnitude as the event-specific warming in Fig. 4d, indicating that the residual ocean dynamical processes play a comparatively minor role. Increases in Q_{net} in the marine heatwave storylines are dominated by larger contributions from net shortwave radiations Q_{SW} and to a smaller extent from evaporative cooling Q_{lat}, as a consequence of a decline in summer low-cloud cover (Fig. 6a). The co-location of low-cloud reductions with the event-specific warming amplification suggests the development of a previously identified positive low-cloud SST feedback[18,19], having the potential to reinforce future summer marine heatwaves in a warmer climate.

In the marine heatwave core, the low-cloud reduction is particularly pronounced, and increases in Q_{SW} drive a dominant positive Flux-varying contribution to the event-specific warming (+0.5 °C, Fig. 5d). This is in part counterbalanced by a negative MLD-varying contribution (−0.3 °C). The particularly shallow MLD in the marine heatwave limits the potential for further shoaling (Fig. 6b). MLD shoaling in the core is thus 50% less than the climatological mean shoaling in the same region and season (Supplementary Fig. 4). This causes the net surface heat flux to be mixed over a volume decreasing less than expected from the mean shoaling trends. The mild warming amplification in the marine heatwave core therefore results from these competing Flux– and MLD–driven effects. In the coastal region and central North Pacific, the event-specific warming amplification is predominantly MLD-driven, contributing by about +0.4 °C (Fig. 5d). Summer MLDs are deeper locally, and storylines exhibit a shoaling about 20% larger than the climatological-mean (Fig. 6b, Supplementary Fig. 4). Surface heat fluxes are thus mixed over a volume decreasing more than expected from the regional-mean shoaling trends, favouring the large warming amplification.

Another prominent feature of the summer 2019 is the reduced anticyclonic surface wind, leading to anomalously northerly winds over the central North Pacific. Air advected from higher latitudes maintains anomalously cold air temperatures in this region (Supplementary Fig. 7). Simulated near-surface winds are virtually indistinguishable in the different climate storylines, due to the wind nudging aloft. However, subpolar regions exhibit a larger surface warming, in agreement with CMIP6 models[43] (Fig. 6c). We thus suggest that projected flux changes in the central North Pacific may also be linked to a reduced cooling effect in the presence of anomalously northerly winds. Indeed, in a +4 °C warmer world, the air mass advected from subpolar regions by the same anomalous northerly winds is subject to a more intense warming than at mid-latitudes, leading to a relatively weaker cooling of the central North Pacific and

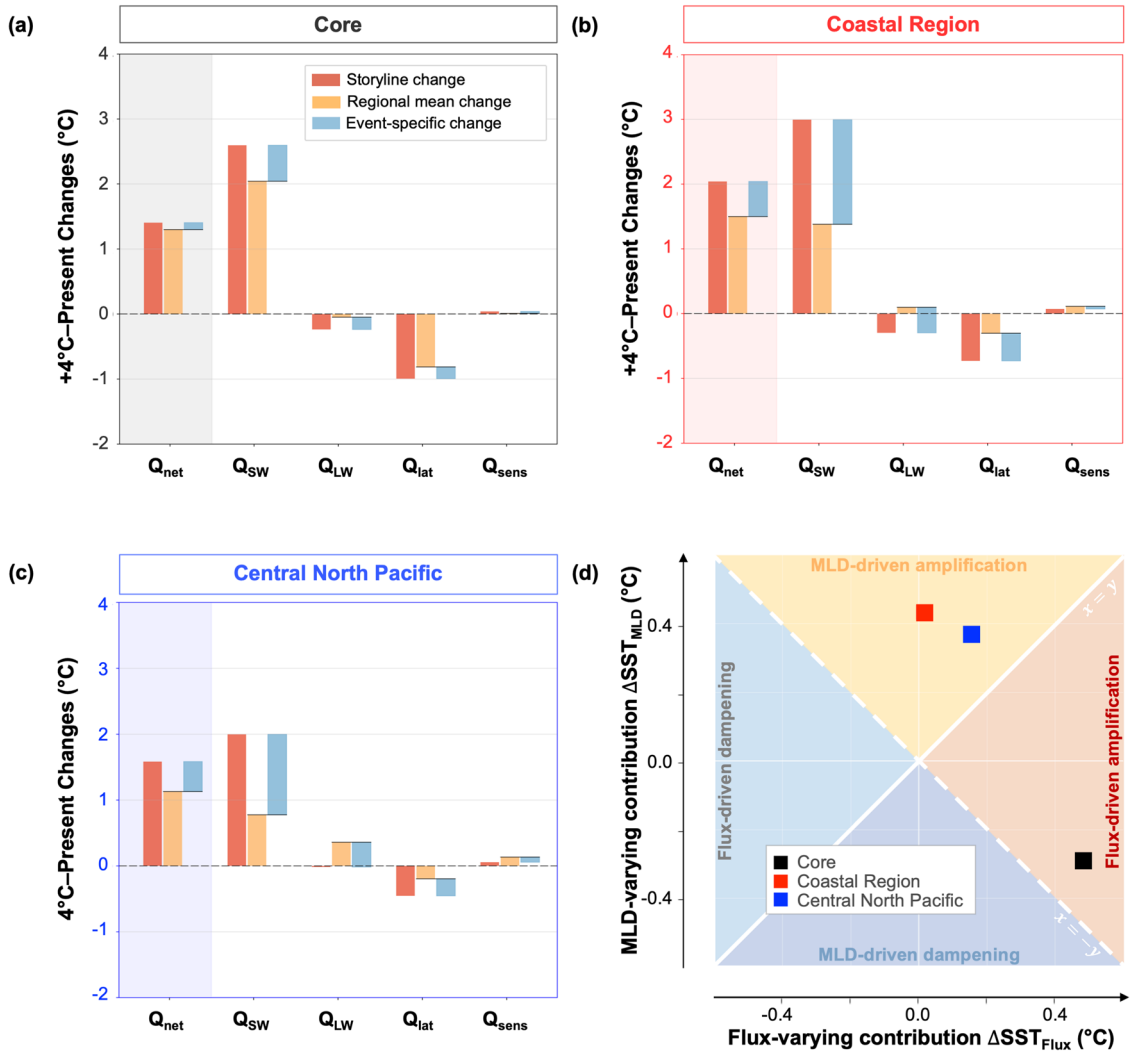

Fig. 5 Projected changes in mixed layer budget-driven warming (°C). Differences between +4 °C and present-day climates, **a** in the marine heatwave core, **b** coastal region and **c** central North Pacific, as defined in Fig. 1. The mixed layer budget-driven warming quantifies how combined changes in both surface heat fluxes and MLD affect the local temperature changes. The storyline change (red bars) is the total marine heatwave change signal, and results from the combined approximate regional mean and event-specific changes (yellow and blue bars respectively). The full mixed layer budget-driven warming from the net surface heat flux absorbed in the mixed layer (Q_{net}, shaded areas) is decomposed into net shortwave radiation, net longwave radiation, latent and sensible heat fluxes (Q_{SW}, Q_{LW}, Q_{lat} and Q_{sens} respectively). **d** Decomposition of the full event-specific budget-driven warming (blue bars in shaded areas in **a**–**c**), into the relative contributions of the event-specific change in net heat flux (Flux-varying contribution ΔSST_{Flux}, x-axis) and of the event-specific change in mixed layer depth (MLD-varying contribution ΔSST_{MLD}, y-axis) to the local temperature change. Their relative amplitude indicates whether event-specific budget-driven warming result from a Flux- or MLD-driven warming dampening or amplification (coloured quadrants). Note that this does not necessarily reflect their absolute importance relative to other terms of the full mixed layer heat budget (e.g., ocean dynamical processes and non-linear terms). Equally reinforcing contributions ($x = y$) and equally counteracting contributions ($x = -y$) are in plain and dashed lines, respectively. Complete analysis is in the Methods.

amplifying heat flux increases. Finally, anomalously southerly winds over the marine heatwave core favour advection of air from subtropical regions undergoing relatively less warming than at mid-latitudes, and may likewise contribute to limit the event-specific warming amplification in the core (Fig. 6c).

Discussion

Despite important impacts on ecosystems, weather, and fishery economics[3–14], understanding how marine heatwaves change in a warming world remains challenging[43,46–48]. The ocean storyline simulations presented in this study can shed new light on the evolution of marine heatwaves and help disentangle the complex interplay between different processes in different climates. To our knowledge, nudged storyline simulations were previously only used for extreme atmospheric events over land[21,32,35]. Here we extend the application of the storyline approach for the first time to an extreme oceanic event. Our coupled climate storyline simulations successfully reproduce the weather-driven Northeast Pacific marine heatwave observed in 2019, generating very close analogues in space and time of the event (Figs. 1 and 2), and therefore confirming that the approach can be used to understand its unfolding in preindustrial (PI), present, and projected +4 °C climates.

Our storyline simulations show that in a PI climate without anthropogenic warming, the summer 2019 atmospheric circulation would have caused Northeast Pacific sea surface temperatures (SSTs) to be 1.4 ± 0.2 °C lower (Fig. 3), exceeding the 1 °C

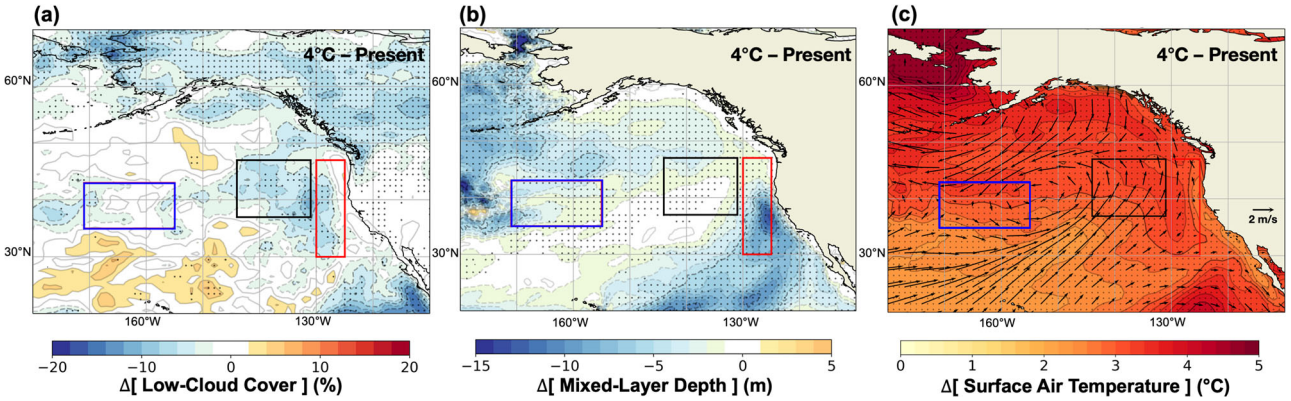

Fig. 6 Drivers of the projected marine heatwave amplification. a Low-cloud cover (%), **b** mixed layer depth (m) and **c** surface air temperature (°C) differences between storyline simulations of the marine heatwave in +4 °C and present-day climates. In **c** vectors of wind anomalies from the present-day nudged storyline simulations (with respect to the simulated 1984–2014 climatology) are in black arrows. Non-overlapping signal between storyline ensemble simulations are in dotted areas. The black, red and blue boxes indicate the marine heatwave core, coastal area, and central North Pacific region.

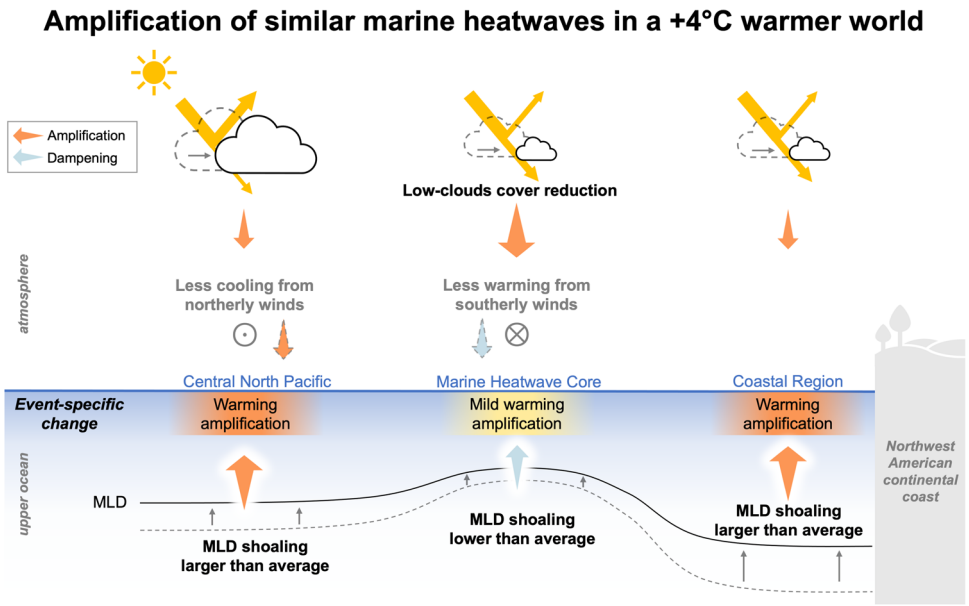

Fig. 7 Projected amplification of future analogues of the summer 2019 Northeast Pacific marine heatwave. Conceptual schematic showing the processes involved in the event-specific warming amplification beyond the projected mean warming, for analogues of the summer 2019 event in a +4 °C climate compared to present-day. The left (right) corresponds to west (east). Changes between present-day (dashed lines) and +4 °C climate (solid lines) conditions are indicated for the low-cloud cover and mixed layer depth (MLD). The amplifying and dampening role of these surface forcing mechanisms on the ocean surface warming are in red and blue arrows, with larger arrows indicating a dominant role on the local amplification. The portion of solar radiation reflected and transmitted by the low clouds is schematized in yellow arrows. Effects of anomalous northerly and southerly winds are in dashed arrows to emphasize that this process is not explicitly quantified in the heat budget analysis.

global ocean warming observed since industrialisation. In a +4 °C climate, a global-mean SST increase of 1.9 °C is projected, yet the increase in future Northeast Pacific marine heatwave analogues may reach 2.9 ± 0.15 °C (+52%). This higher warming signal results to a large part from processes specific to this marine heatwave that further amplify SSTs beyond the projected regional mean warming (Fig. 4). Overall, our results suggest that event-specific processes tend to laterally extend marine heatwave in a warming climate while having limited effects on core warming.

Adapting the mixed layer heat budget[1,47–50] to our storyline simulations, we quantify contributions to these marine heatwave-specific temperature changes (Figs. 5 and 6). We identify three important drivers of the projected marine heatwave warming amplification: shoaling of the ocean-mixed layer, changes in the low-cloud cover and relative warming of air advected by the anomalous winds. The interplay between these surface forcing processes varies between the three regions of interest in the marine heatwave (core, coast, and central North Pacific), counteracting or reinforcing one another locally (Fig. 7).

Some challenges remain regarding our understanding of the drivers of event-specific changes. For example, our results suggest that ocean dynamical processes likely remain important in dampening the PI–to–present warming, while changes in surface forcing processes primarily drive the warming amplification in a future +4 °C world. This dichotomous warming response in PI–to–present and present–to–+4 °C climates merits further investigation. Relatively deeper mixed layers in a PI climate may favour larger contributions from horizontal ocean advection, in particular by large-scale currents such as the Kuroshio Extension or the California Current[47,51]. Near the coast, under the summer

2019 weaker-than-usual northerly wind conditions, a possible breakdown of the eastern-boundary upwelling system which normally cools the surface[52] could explain the projected faster-than-average coastal warming rate, while opposing the dampened warming signal between present and PI storylines. Changing effects of local land-ocean-atmosphere interactions[53] and remote SST forcings[1,54] in a warming world should also be considered. Moreover, small-scale ocean features can play an important role in setting marine heatwave characteristics[14,51] but are not resolved in our medium-resolution simulations. Investigating the contribution of vertical and lateral eddy fluxes to marine heatwaves in a changing climate would require eddy-resolving ocean resolutions.

Potential changes in likelihood of the summer 2019 atmospheric are not addressed by storyline simulations, which could appear at first as a limitation of our approach. Yet, in doing so, the storylines circumvent the large uncertainties related to the response of atmospheric dynamics and variability to climate change[55,56] and complement the traditional statistical approach by isolating thermodynamical-only changes. Additionally, there is evidence that the ongoing and projected strong Arctic warming favours the prevalence of atmospheric patterns similar to those responsible for the 2019 Northeast Pacific marine heatwave[57]. Analogues of this marine heatwave thus remain dynamically plausible in a warmer world, confirming the robustness of our storyline-based analysis.

Extending our case study to other marine heatwaves could provide insights on how the local response to climate change may vary in different regions and seasons. Air temperature advection, for example, is likely to vary with regional and atmospheric configurations. On the other hand, the mixed layer depth (MLD) is expected to continue shoaling globally as a result of the long-term surface warming[48], and will likely affect temperature extremes in most of the world's oceans. Here one can argue that the reduced ocean MLD acts similarly to low soil moisture conditions for continental heatwaves[20,21]: reductions in ocean MLD and soil moisture can both enhance temperature variability and warm extremes[48,58], but both can also experience saturation effects that limit further process-driven temperature amplification. A complete MLD shoaling up to the surface implies a fast response to atmospheric temperatures, while total soil drying implies the loss of evaporative cooling. Similarly, reduced low-cloud cover in response to warming is a typical component of the positive extratropical marine cloud feedback in models and observations[59], and is expected to generally amplify extratropical marine heatwaves. In the sub-tropical trade wind regions, some models overestimate the reduction of low clouds under warming[60] and thereby the positive cloud feedback, thus likely overestimating the amplification of future marine heatwaves. Finally, quantifying the ecological and biogeochemical impacts of marine heatwaves[3,14] may reveal important non-linear responses, for instance affecting temperature-sensitive species such as corals, or the solubility of carbon dioxide in seawater.

Our findings show the potential of the nudged storyline approach as a reference for other heatwaves globally. Multiple intense marine heatwaves have been reported worldwide in summer 2022, including the resurgence of warm anomalies in the North Pacific Ocean and record-high temperatures in the Mediterranean Sea. Our Northeast Pacific case study suggests that in an even warmer climate, future marine heatwave temperatures may warm faster than the global and regional mean temperature. Further process-based assessments of marine heatwaves and their drivers, similar to their atmospheric and land counterparts, will be instrumental in improving marine heatwave projection.

Methods

Nudged simulations. We use simulations based on AWI-CM-1-1-MR[39–41] (AWI-CM-1 throughout the paper). This coupled climate model has contributed to the phase 6 of the Coupled Model Intercomparison Project (CMIP6[42]) and employs the atmospheric model ECHAM6.3.04p1 from MPI-M[61] for the atmospheric component, and the Finite Element Sea Ice–Ocean Model (FESOM) v.1.4[62] for the ocean component. The atmosphere component is run at a T127L95 spectral resolution (~100 km), with 95 vertical levels going up to ~0.01 hPa. The ocean model FESOM uses an unstructured mesh allowing a refined resolution for example in eddy-rich regions, ranging here from 80 km in the subtropical Pacific, 30–60 km in the Northeast Pacific, and down to 8 km in the Gulf Stream area[39].

The observed atmospheric circulation is constrained by nudging the model's vorticity and divergence with a relaxation timescale of 24 h and a spectral truncation of 20 on zonal wavenumbers. Only vertical levels between 700 hPa and 100 hPa are nudged. This configuration has been shown to optimally constrain atmospheric patterns at scales larger than ~2000 km, while preserving some freedom in the boundary layer and at small spatiotemporal time-scales[21]. Based on this configuration, storyline simulations are run in different climates, nudged to the ERA5[63] dynamical atmospheric conditions starting on the 1st January 2017 until the 31st December 2020. Storylines are initialised using states from our AWI-CM-1 historical and Shared Socio-economic Pathway scenario ssp370 free-running simulations[21] to produce the different background climate conditions. Preindustrial, present-day and +4 °C conditions are obtained by branching 4-year nudged simulations off the free runs respectively on the 1st January 1851, 2017 and 2093, the latter corresponding to a +4 °C global mean surface air temperature increase compared to preindustrial in the model. In the global ocean, a +4 °C world amounts to an annual and summer mean SST increase of 1.9 °C compared to present-day conditions (and 2.9 °C compared to preindustrial). The nudged simulations are extended from these initial states and use the transient historical and scenario forcing corresponding to the four years following the date at which they are branched off. Therefore, the nudged storylines of the summer 2019 marine heatwave correspond to the same imposed (nudged) year 2019 wind conditions if they occurred in the climate conditions of year 1853 (preindustrial storylines), 2019 (present-day storylines), and 2095 (4 °C warmer storylines). Storylines each comprise five 4-year ensemble members spawned from the five respective free-running simulation ensemble members and thus starting from different initial conditions. Figures show ensemble means for each five-member storyline ensemble.

SST anomalies. SST anomalies (SSTAs) shown in Fig. 1 are derived with respect to a common reference period 1984–2014. Anomalies for the reanalysis fields are produced with respect to the ERA5 climatology. For nudged storylines, we derive the simulated climatology from the 5-member ensemble mean of our AWI-CM-1 free-running simulations, from which the storylines are branched off. We then compute the storyline SSTAs in pre-industrial, present-day and +4 °C climates all with respect to the simulated 1984–2014 climatology. The SSTAs obtained in this manner were then used to compute the correlation coefficient between ERA5 and present-day storyline time-series.

Climatological-mean states. Mean states for different climates are derived from the 5-member ensemble AWI-CM-1-MR free-running simulations. Climatological-mean states are obtained by

performing multi-year daily averages over 10-year windows for the preindustrial, present-day, and +4 °C climates, respectively, 1850–1859, 2015–2024, and 2091–2100.

Storyline, regional mean, and event-specific changes. For a given parameter, the storyline change is the difference between the summer-season, 5-member ensemble means of two storylines in different climates. Similarly, the climatological long-term summer mean change is the difference between climatological-mean states corresponding to preindustrial, present-day or +4 °C climates. The climatological global-mean summer SST increase is referred to as the GMSST increase. The field of climatological summer mean warming focused on a chosen subregion is referred to as the regional mean warming. To discriminate the long-term regional mean warming from warming that is specific to the summer 2019 Northeast Pacific atmospheric circulation, the storyline warming between different climates is compared to the regional mean warming. The regional mean warming field is subtracted from the storyline warming, resulting in the so-called field of event-specific change. A positive event-specific SST change, indicating a larger warming in storylines than in climatological means, is called warming amplification. Inversely, a negative event-specific SST change is called warming dampening.

Non-overlapping signal. In this study, non-overlapping storyline ensembles highlight changes in our simulations with a particularly high signal-to-noise ratio. At a given grid point, the lack of overlap between the two 5-member storyline ensembles being compared (i.e., present-day against preindustrial storylines or +4 °C against present-day storylines) indicates that the sign of the storyline warming is consistent across all member-wise differences. This criterion corresponds to a p-value of 0.008 according to a two-sided Mann–Whitney test, thus statistically very strict. Similarly, absence of overlap between storyline warming and regional mean warming means that the storyline signal is consistently larger (lower) than the regional mean warming across all member-wise differences, and indicates a particularly strong event-specific amplification (dampening) signal.

Confidence intervals. Storyline, regional mean, and event-specific warming rates are provided with a one standard error interval (corresponding to a confidence interval of 68%). Standard errors (SE) of each n-member ensemble is computed such as $SE = \frac{\sigma}{\sqrt{n}}$, where σ is the n-member ensemble standard deviation normalised by n−1. Standard errors are propagated for differences between a climate a and a climate b, such as: $SE_\Delta = \sqrt{SE_a{}^2 + SE_b{}^2}$,

Heat budget analysis. We distinguish the total signal during the extreme event (storyline signal, noted total hereafter), as the sum of two components: (i) the regional (and seasonal-) long-term mean signal (regional mean, noted bar $\overline{\ }$); and (ii) the event-specific anomalies departing from the mean signal (noted SSTA or prime $'$ for other parameters). Following this convention, we define the total temperature tendency $\Delta_t SST^{total}$ during the marine heatwave, i.e, the difference between temperatures at the start (here, May-average) and peak (August-average) of the marine heatwave[1], such as:

$$\Delta_t SST^{total} = \overline{\Delta_t SST} + \Delta_t SSTA \quad (1)$$

Where $\overline{\Delta_t SST}$ is the climatological mean temperature tendency (i.e., the seasonal signal in a given climate) and $\Delta_t SSTA$ is the anomalous temperature tendency during the event, superimposed to the seasonal signal. We assume the mixed layer depth and sea surface temperatures vary together in the model.

Following previous studies[1,47,50], we derive the simplified mixed layer temperature heat budget during the marine heatwave:

$$\Delta_t SST^{total} = \frac{1}{\rho C_p}\frac{Q_{net}{}^{total}}{MLD^{total}} + \varepsilon_0 \quad (2)$$

The first right-hand side term represents the contribution of the surface heat fluxes absorbed in the mixed-layer to the total temperature tendency $\Delta_t SST^{total}$. Here, ρ is the density of seawater, C_p the specific heat capacity at constant pressure, $Q_{net}{}^{total}$ is the net surface heat flux (into the mixed layer) and MLD^{total} the MLD during the marine heatwave event. The term ε_0 is a residual term including both the oceanic advection and vertical entrainment. The dynamical oceanic term ε_0 in equation is usually small compared to the contribution of surface forcing processes, especially in regions with shallow MLD (Amaya et al. 2020, Takahashi et al. 2023). In the following, we thus only derive explicitly the mixed layer budget-driven warming resulting from changes in surface heat fluxes absorbed in the mixed layer, that is, the first right-hand side term.

We consider differences Δ_b^a between a climate a and a climate b (which can be present-day and preindustrial climates, or +4 °C warmer and present-day, respectively). There is an event-specific warming amplification if the total temperature tendency during the event $\Delta_t SST^{total}$ increases more than the regional mean climatological temperature tendency (i.e., the change in seasonal signal) $\overline{\Delta_t SST}$, and vice-versa for a warming dampening, such as:

$$\Delta_b^a \Delta_t SSTA = \Delta_b^a \Delta_t SST^{total} - \Delta_b^a \overline{\Delta_t SST}$$
$$\Delta_b^a \Delta_t SSTA \begin{cases} >0, \text{warming amplification} \\ <0, \text{warming dampening} \end{cases} \quad (3)$$

Considering only the mixed layer budget-driven warming resulting from changes in surface forcing processes, $\Delta_b^a \Delta_t SST^{total}$ is derived from the storyline signal using the first right-hand side term of Eq. (2). First order effects of $\Delta_b^a \overline{\Delta_t SST}$ are represented here by $\frac{1}{\rho C_p}\Delta_b^a\left(\frac{\overline{Q_{net}}}{\overline{MLD}}\right)$, i.e., the temperature change between mean climate a conditions and mean climate b conditions. We therefore estimate the anomalous event-specific change in Eq. (3) as:

$$\Delta_b^a \Delta_t SSTA \approx \frac{1}{\rho C_p}\Delta_b^a\left(\frac{Q_{net}{}^{total}}{MLD^{total}}\right) - \frac{1}{\rho C_p}\Delta_b^a\left(\frac{\overline{Q_{net}}}{\overline{MLD}}\right) \quad (4)$$

Where both right hand-side terms represent the mixed layer budget-driven temperature change, that is, the contribution of changes in surface heat flux and MLD to changes in the temperature tendency. The first right hand-side term corresponds to storyline changes, and the second right hand-side term corresponds to regional mean climatological changes.

We decompose the changes in mixed layer heat budget into contributions from each fluxes, such as:

$$Q_{net} = Q_{SW} + Q_{LW} + Q_{lat} + Q_{sens} \quad (5)$$

Where Q_{SW} is the net shortwave radiation minus the penetrative shortwave radiation at the bottom of the mixed layer[64], Q_{LW} the net longwave radiation, Q_{lat} the latent heat flux and Q_{sens} the sensible heat flux. By computing the terms of Eq. (4) for each flux of Eq. (5), we quantify the contribution of each flux change to changes in mixed layer budget-driven temperature change (Fig. 5a–c). Note that budget terms are multiplied by three months (the duration of the marine heatwave onset) to convert to degree units[1].

Based on Eq. (4), the event-specific budget-driven temperature change resulting from anomalous changes in net surface heat flux

absorbed in the mixed layer (blue bars in Fig. 5a–c) can be reformulated into:

$$\Delta_b^a \Delta_t SSTA \approx \frac{1}{\rho C_P} \Delta_b^a \left(\frac{Q_{net}{}^{total}}{MLD^{total}} - \frac{\overline{Q_{net}}}{\overline{MLD}} \right) \approx \frac{1}{\rho C_P} \Delta_b^a \left(\frac{Q_{net}}{MLD} \right)' \quad (6)$$

Expanding on previous work[1,17,49,50], we determine the dominant drivers of the event-specific budget-driven temperature change by decomposing Q_{net} and MLD terms into their mean (noted bar $\overline{\ }$) and event-specific anomaly (noted prime′) components. We develop Eq. (6) using the Taylor expansion and linearising[50] into:

$$\frac{1}{\rho C_P} \Delta_b^a \left(\frac{Q_{net}}{MLD} \right)' \approx \frac{1}{\rho C_P} \Delta_b^a \left(\frac{Q_{net}{}'}{\overline{MLD}} \right) - \frac{1}{\rho C_P} \Delta_b^a \left(\frac{\overline{Q_{net}} MLD'}{\overline{MLD}^2} \right) \quad (7)$$

The term on the left-hand side of Eq. (7) is the full contribution of event-specific change in mixed layer heat budget to the local temperature change, comprising event-specific changes in both surface heat flux and MLD. The first term on the right-hand side quantifies changes in mixed layer heat budget due to event-specific changes in surface heat flux only (referred to as the Flux-varying contribution and noted ΔSST_{Flux}). It represents the event-specific temperature increase that result from changes in event-specific surface heat fluxes if they were mixed over mean MLDs in their respective climates. The second term on the right-hand side quantifies changes due to event-specific changes in MLD only (referred to as the MLD-varying contribution and noted ΔSST_{MLD}). It represents the event-specific temperature increase that result from changes in mean surface heat fluxes if they were mixed over event-specific MLDs in their respective climates.

Depending on the relative amplitude and sign of the respective contributions, we can determine the nature of the temperature change associated with event-specific changes in net surface heat flux absorbed in the mixed layer (Fig. 5d, Supplementary Fig. 5d), where bars denote absolute amplitude values:

$$\begin{cases} \Delta SST_{MLD} > 0 \text{ and } |\Delta SST_{MLD}| > |\Delta SST_{Flux}|: & \text{MLD} - \text{driven amplification} \\ \Delta SST_{Flux} > 0 \text{ and } |\Delta SST_{Flux}| > |\Delta SST_{MLD}|: & \text{Flux} - \text{driven amplification} \\ \Delta SST_{MLD} < 0 \text{ and } |\Delta SST_{MLD}| > |\Delta SST_{Flux}|: & \text{MLD} - \text{driven dampening} \\ \Delta SST_{Flux} < 0 \text{ and } |\Delta SST_{Flux}| > |\Delta SST_{MLD}|: & \text{Flux} - \text{driven dampening} \end{cases} \quad (8)$$

Data availability

Data from the AWI-CM-1-1-MR free runs are available in the Earth System Grid Federation (ESGF) data nodes (https://esgf-data.dkrz.de/search/cmip6-dkrz/). The nudged storyline simulations are stored in the supercomputer Levante from DKRZ and are available online (Zenodo, DOI: https://doi.org/10.5281/zenodo.10401040). ERA5 reanalysis data used in this study can be accessed from the European Centre for Medium-Range Weather Forecasts (ECMWF; https://www.ecmwf.int/en/forecasts/datasets/reanalysis-datasets/era5).

Code availability

The source code for the coupled FESOM v.1.4 model that is used in AWI-CM-1-1-MR is available online (Zenodo, https://doi.org/10.5281/zenodo.10401309). For the source code of ECHAM6, registration on the MPI-ESM user page is required (http://www.mpimet.mpg.de/en/science/models/license/).

Received: 17 May 2023; Accepted: 10 January 2024;
Published online: 26 January 2024

References

1. Amaya, D. J. et al. Physical drivers of the summer 2019 North Pacific marine heatwave. *Nat. Commun.* **11**, 1903 (2020).
2. Bond, N. A., Cronin, M. F., Freeland, H. & Mantua, N. Causes and impacts of the 2014 warm anomaly in the NE Pacific. *Geophys. Res. Lett.* **42**, 3414–3420 (2015).
3. Cavole, L. M. et al. Biological impacts of the 2013–2015 warm-water anomaly in the Northeast pacific: winners, losers, and the future. *Oceanography* **29**, 273–285 (2016).
4. Jones, T. et al. Massive mortality of a planktivorous seabird in response to a marine heatwave. *Geophys. Res. Lett.* **45**, 3193–3202 (2018).
5. Piatt, J. F. et al. Extreme mortality and reproductive failure of common murres resulting from the Northeast Pacific marine heatwave of 2014–2016. *PLOS ONE* **15**, e0226087 (2020).
6. Gabriele, C. M. et al. Sharp decline in humpback whale (Megaptera novaeangliae) survival and reproductive success in southeastern Alaska during and after the 2014–2016 Northeast Pacific marine heatwave. *Mamm. Biol.* https://doi.org/10.1007/s42991-021-00187-2 (2022).
7. Seager, R. et al. Causes of the 2011–14 California Drought. *J. Clim.* **28**, 6997–7024, (2015).
8. Di Lorenzo, E. & Mantua, N. Multi-year persistence of the 2014/15 North pacific marine heatwave. *Nat. Clim. Change* **6**, 1042–1047 (2016).
9. Szuwalski, C. S., Aydin, K., Fedewa, E. J., Garber-Yonts, B. & Litzow, M. A. The collapse of eastern Bering Sea snow crab. *Science* **382**, 306–310 (2023).
10. Laurel, B. J. & Rogers, L. A. Loss of spawning habitat and prerecruits of Pacific cod during a Gulf of Alaska heatwave. *Can. J. Fisheries Aquatic Sci.* **77**, 644–650 (2020).
11. von Biela, V. R. et al. Premature Mortality Observations among Alaska's Pacific Salmon During Record Heat and Drought in 2019. *Fisheries* **47**, 157–168 (2022).
12. Jones, T. et al. Marine bird mass mortality events as an indicator of the impacts of ocean warming. *Mar. Ecol. Prog. Ser.* HEATav8. https://doi.org/10.3354/meps14330 (2023)
13. IPCC, 2019: IPCC Special Report on the Ocean and Cryosphere in a Changing Climate [H.-O. Pörtner, et al. (eds.)]. Cambridge University Press, Cambridge, UK and New York, NY, USA, 755
14. Guo, X. et al. Threat by marine heatwaves to adaptive large marine ecosystems in an eddy-resolving model. *Nat. Clim. Chang.* **12**, 179–186 (2022).
15. Amaya, D. J. The Pacific Meridional Mode and ENSO: a Review. *Curr. Clim. Change Rep* **5**, 296–307 (2019).
16. Sen Gupta, A. et al. Drivers and impacts of the most extreme marine heatwave events. *Sci. Rep.* **10**, 19359 (2020).
17. Amaya, D. J., et al. Are long-term changes in mixed layer depth influencing North Pacific marine heatwaves? *Bull. Am. Meteorol. Soc.* 102. https://doi.org/10.1175/BAMS-D-20-0144.1 (2021)
18. Norris, J. R., Zhang, Y. & Wallace, J. M. Role of low clouds in summertime atmosphere-ocean interactions over the North Pacific. *J. Clim.* **11**, 2482–2490 (1998).
19. Klein, S. A. et al. Low-Cloud Feedbacks from Cloud-Controlling Factors: A Review. *Surv. Geophys.* **38**, 1307–1329 (2017).
20. Selten, F. M. et al. Future continental summer warming constrained by the present-day seasonal cycle of surface hydrology. *Sci. Rep.* **10**, 4721 (2020).
21. Sánchez-Benítez, A., Goessling, H., Pithan, F., Semmler, T. & Jung, T. The July 2019 European Heat Wave in a Warmer Climate: Storyline Scenarios with a Coupled Model Using Spectral Nudging. *J. Clim.* **35**, 2373–2390, (2022).
22. Oliver, E. C. J. et al. Longer and more frequent marine heatwaves over the past century. *Nat. Commun.* **9**, 1324 (2018).
23. Frölicher, T. L. & Laufkötter, C. Emerging risks from marine heat waves. *Nat. Commun.* **9**, 650 (2018).
24. Laufkötter, C., Zscheischler, J. & Frölicher, T. L. High-impact marine heatwaves attributable to human-induced global warming. *Science* **369**, 1621–1625 (2020).
25. Barkhordarian, A., Nielsen, D. M. & Baehr, J. Recent marine heatwaves in the North Pacific warming pool can be attributed to rising atmospheric levels of greenhouse gases. *Commun. Earth Environ.* **3**, 131 (2022).
26. Scannell, H. A. et al. Frequency of marine heatwaves in the North Atlantic and North Pacific since 1950. *Geophys. Res. Lett.* **43**, 2069–2076 (2016).
27. Joh, Y. & Di Lorenzo, E. Increasing coupling between NPGO and PDO leads to prolonged marine heatwaves in the Northeast pacific. *Geophys. Res. Lett.* **44**, 11–663 (2017).
28. Oliver, E. C. J. Mean warming not variability drives marine heatwave trends. *Clim. Dyn.* **53**, 1653–1659 (2019).
29. Philip, S. et al. A protocol for probabilistic extreme event attribution analyses. *Adv. Stat. Climatol. Meteorol. Oceanogr.* **6**, 177–203 (2020).
30. Suarez-Gutierrez, L., Milinski, S. & Maher, N. Exploiting large ensembles for a better yet simpler climate model evaluation. *Clim. Dyn.* **57**, 2557–2580 (2021).
31. Shepherd, T. G. A common framework for approaches to extreme event attribution. *Curr. Clim. Change Rep.* **2**, 28–38 (2016).

32. van Garderen, L. & Mindlin, J. A storyline attribution of the 2011/2012 drought in Southeastern South America. *Weather* **77**, 212–218 (2022).
33. Schubert-Frisius, M., Feser, F., von Storch, H. & Rast, S. Optimal Spectral Nudging for Global Dynamic Downscaling. *Monthly Weather Rev.* **145**, 909–927, (2017).
34. Shepherd, T. G. et al. Storylines: An alternative approach to representing uncertainty in physical aspects of climate change. *Clim. Change* **151**, 555–571 (2018).
35. Wehrli, K., Hauser, M. & Seneviratne, S. I. Storylines of the 2018 Northern Hemisphere heatwave at preindustrial and higher global warming levels. *Earth Syst. Dyn.* **11**, 855–873 (2020).
36. Shepherd, T. G. Atmospheric circulation as a source of uncertainty in climate change projections. *Nat. Geosci.* **7**, 703–708 (2014).
37. Hoskins, B. & Woollings, T. Persistent extratropical regimes and climate extremes. *Curr. Clim. Change Rep.* **1**, 115–124 (2015).
38. Woollings, T. et al. Blocking and its response to climate change. *Curr. Clim. Change Rep.* **4**, 287–300 (2018).
39. Sidorenko, D. et al. Towards multi-resolution global climate modeling with ECHAM6–FESOM. Part I: Model formulation and mean climate. *Clim. Dyn.* **44**, 757–780 (2015).
40. Rackow, T. et al. Towards multi-resolution global climate modeling with ECHAM6-FESOM. Part II: climate variability. *Clim. Dyn.* **50**, 2369–2394 (2018).
41. Semmler, T. et al. Simulations for CMIP6 with the AWI climate model AWI-CM-1-1. *J. Adv. Model. Earth Syst.* **12**, e2019MS002009 (2020).
42. Eyring, V. et al. Overview of the Coupled Model Intercomparison Project Phase 6 (CMIP6) experimental design and organization. *Geosci. Model Dev.* **9**, 1937–1958 (2016).
43. IPCC, 2021. *Climate Change 2021: The Physical Science Basis. Contribution of Working Group I to the Sixth Assessment Report of the Intergovernmental Panel on Climate Change* (eds. Masson-Delmotte, V., et al.) 2391 (Cambridge University Press, Cambridge, United Kingdom and New York, NY, USA, 2021).
44. Merrifield, A. L., Brunner, L., Lorenz, R., Humphrey, V. & Knutti, R. Climate model Selection by Independence, Performance, and Spread (ClimSIPS v1.0.1) for regional applications. *Geosci. Model Dev.* **16**, 4715–4747 (2023).
45. van Garderen, L., Feser, F. & Shepherd, T. G. A methodology for attributing the role of climate change in extreme events: a global spectrally nudged storyline. *Nat. Hazards Earth Syst. Sci.* **21**, 171–186 (2021).
46. Plecha, S. M. & Soares, P. M. Global marine heatwave events using the new CMIP6 multi-model ensemble: from shortcomings in present climate to future projections. *Environ. Res. Lett.* **15**, 124058 (2020).
47. Holbrook, N. J. et al. A global assessment of marine heatwaves and their drivers. *Nat. Commun.* **10**, 2624 (2019).
48. Shi, H. et al. Global decline in ocean memory over the 21st century. *Sci. Adv.* **8**, eabm3468 (2022).
49. Takahashi, N. et al. Observed relative contributions of anomalous heat fluxes and effective heat capacity to sea surface temperature variability. *Geophys. Res. Lett.* **50**, e2023GL103165 (2023).
50. Alexander, M. A. & Penland, C. Variability in a mixed layer ocean model driven by stochastic atmospheric forcing. *J. Clim.* **9**, 2424–2442 (1996).
51. Bian, C. et al. Oceanic mesoscale eddies as crucial drivers of global marine heatwaves. *Nat. Commun.* **14**, 2970 (2023).
52. Wang, S. et al. Southern hemisphere eastern boundary upwelling systems emerging as future marine heatwave hotspots under greenhouse warming. *Nat. Commun.* **14**, 28 (2023).
53. Hu, L. A global assessment of coastal marine heatwaves and their relation with coastal urban thermal changes. *Geophys. Res. Lett.* **48**, e2021GL093260 (2021).
54. Silva, E. N. S. & Anderson, B. T. Northeast Pacific marine heatwaves linked to Kuroshio Extension variability. *Commun. Earth Environ.* **4**, 367 (2023).
55. Screen, J. Arctic amplification decreases temperature variance in Northern mid- to high-latitudes. *Nat. Clim. Change* **4**, 577–582 (2014).
56. Brewer, M. C. & Mass, C. F. Projected Changes in Western U.S. Large-Scale Summer Synoptic Circulations and Variability in CMIP5 Models. *J. Clim.* **29**, 5965–5978, (2016).
57. Song, S. Y. et al. Arctic warming contributes to increase in Northeast Pacific marine heatwave days over the past decades. *Commun. Earth Environ.* **4**, 25 (2023).
58. Seneviratne, S. I. et al. Investigating soil moisture–climate interactions in a changing climate: A review. *Earth Sci. Rev.* **99**, 125–161 (2010).
59. Myers, T. A. et al. Observational constraints on low cloud feedback reduce uncertainty of climate sensitivity. *Nat. Clim. Chang.* **11**, 501–507 (2021).
60. Vogel, R. et al. Strong cloud–circulation coupling explains weak trade cumulus feedback. *Nature* **612**, 696–700 (2022).
61. Stevens, B. et al. Atmospheric component of the MPI-M earth system model: ECHAM6. *J. Adv. Model. Earth Syst.* **5**, 146–172 (2013).
62. Wang, Q. et al. The Finite Element Sea Ice-Ocean Model (FESOM) v.1.4: Formulation of an ocean general circulation model. *Geosci. Model Dev.* **7**, 663–693 (2014).
63. Hersbach, H. et al. The ERA5 global reanalysis. *Q. J. R. Meteorol. Soc.* **146**, 1999–2049 (2020).
64. Morel, A. & Antoine, D. Heating rate within the upper ocean in relation to its bio–optical state. *J. Phys. Oceanogr.* **24**, 1652–1665 (1994).
65. Barbi, D. et al. ESM-Tools version 5.0: a modular infrastructure for stand-alone and coupled Earth system modelling (ESM). *Geosci. Model Dev.* **14**, 4051–4067 (2021).

Acknowledgements

This work was supported by funding from the Federal Ministry of Education and Research (BMBF) and the Helmholtz Research Field Earth & Environment for the Innovation Pool Project SCENIC. Initial storyline simulations were also supported through funding from the Helmholtz-Climate-Initiative for the HI-CAM project. M.A. and H.F.G. received funding from the Federal Ministry of Education and Research of Germany in the framework of SSIP (Seamless Sea Ice Prediction; grant no. 01LN1701A). A. S.-B. was supported by funding from the Innovation Pool Project SCENIC. All simulations were performed at the German Climate Computing Center (DKRZ) using ESM Tools[65]. We thank Dmitry Sidorenko for supporting the penetrative shortwave radiation calculations.

Author contributions

M.A. wrote the initial manuscript and designed the study together with H.F.G. and T.J. A.S.-B. conducted the model experiments and processed the data. M.A. analysed the results. F.P. added the discussion on marine cloud feedbacks. All authors contributed to the discussions and reviewed the manuscript.

Funding

Open Access funding enabled and organized by Projekt DEAL.

Competing interests

The authors declare no competing interests.

Additional information

Supplementary information The online version contains supplementary material available at https://doi.org/10.1038/s43247-024-01212-1.

Correspondence and requests for materials should be addressed to Marylou Athanase.

Peer review information *Communications Earth & Environment* thanks Toru Miyama and the other, anonymous, reviewer(s) for their contribution to the peer review of this work. Primary Handling Editors: Regina Rodrigues, Clare Davis and Aliénor Lavergne. A peer review file is available.